Heliyon 10 (2024) e37029

Contents lists available at ScienceDirect

Heliyon

journal homepage: www.cell.com/heliyon

Research article

A study on properties of electroless Ni-B/MgB_2 coatings on AZ91 magnesium alloy

Ferhat Bülbül *, Tuğçenur Kılcı

Department of Mechanical Engineering, Erzurum Technical University, Erzurum, 25050, Turkiye

ARTICLE INFO

Keywords:
MgB_2
Electroless deposition
Composite coating
Ni-B

ABSTRACT

This study explores MgB_2 as a reinforcing agent in electroless deposition on AZ91 magnesium alloy substrates, evaluating its impact on coating properties. X-ray diffraction (XRD) analysis shows that the amorphous Ni-B coating masks initial magnesium peaks, while MgB_2 enhances $MgB_2O(OH)_6$, MgB_2O_5, MgO, and $MgB_{2x}Oy$ oxide phases. SEM images illustrate morphological shifts from cauliflower-like Ni-B structures to dendritic and fibrous MgB_2 forms, with higher MgB_2 concentrations leading to granular structures with randomly oriented crystallites resembling platelets, indicating increased magnesium content. MgB_2-reinforced Ni-B coatings exhibited higher hardness than the substrate but lower than as-deposited Ni-B. Friction coefficients initially decreased with Ni-B, increased significantly with 0.1 g MgB_2, and decreased with higher reinforcements, remaining higher than substrate and as-deposited Ni-B. MgB_2 reinforcement increased surface roughness, causing local agglomerations in 0.5 g MgB_2 coatings. Contact angle measurements demonstrated enhanced hydrophilicity due to MgB_2's superhydrophilic properties influenced by surface roughness. Antibacterial tests revealed superior properties with 0.1 g MgB_2, suggesting a transition to MgB_2-enriched structures and influencing material properties. While Ni-B/MgB_2 coatings improved over substrate, further research is needed to optimize parameters and understand stabilizer effects. These coatings also exhibited superhydrophilicity and promising antibacterial properties, suggesting potential in advanced surface engineering applications.

1. Introduction

Magnesium and its alloys have garnered significant interest due to their exceptional properties [1,2]. Various methods have been employed to enhance the surface characteristics of magnesium alloys. Anodizing stands out as a potential method for protecting magnesium alloy surfaces. However, traditional methods like anodizing, though effective, often involve hazardous components such as fluorides and chromates. In recent years, environmentally friendly alternatives such as electroless plating have gained popularity for their cost-effectiveness and ability to provide superior hard coatings with excellent wear resistance and natural lubricity properties compared to electroplated nickel and hard chrome [3,4]. Electroless plating is an autocatalytic process where metal ions in aqueous solutions deposit onto a substrate without the need for an electric current, forming a thin metallic layer through oxidation-reduction reactions [5–7]. Incorporating second-phase particles into nickel-based matrices to create composite coatings has been a promising strategy to enhance corrosion and wear resistance [8,9]. These particles can include ceramic compounds such as SiO_2 [10–14], SiC [15–20], B_4C [21–25], TaC [26], TiC [27], Si_3N_4 [28–31], Fe_3O_4 [32], ZnO [33], ZrO_2 [34], TiO_2 [14,35–39], Al_2O_3 [14,40–43], CeO_2

* Corresponding author.
E-mail addresses: ferhat.bulbul@erzurum.edu.tr (F. Bülbül), tugce.kilci8@gmail.com (T. Kılcı).

https://doi.org/10.1016/j.heliyon.2024.e37029
Received 25 August 2023; Received in revised form 14 August 2024; Accepted 26 August 2024
Available online 30 August 2024

[44–46], and CuO [14], in either amorphous or crystalline forms within the nickel-based matrix, however, MgB_2 particles have not been explored. The ceramic particles used in the studies cited above have provided benefits in terms of mechanical (hardness) and tribological properties for electroless Ni-B coatings. Bülbül et al. [47,48] produced MgB_2 not as a reinforcement but as a direct coating material in both spray pyrolysis and electroless deposition processes, achieving more durable and superhydrophilic MgB_2 surfaces on metallic substrates. Furthermore, Vijayaragavan et al. [49] applied the electroless coating method to fabricate MgB_2 coatings, specifically not as a reinforcing component. Their objective was to enhance the superconducting characteristics of substate materials such as silver, gold, and silicon with this ceramic structure (see Table 1).

The novelty of this study lies in the utilization of magnesium diboride (MgB_2) as a reinforcing phase in electroless nickel-boron (Ni-B) alloy coatings, aimed specifically at enhancing their mechanical and frictional properties. Although MgB_2 is well-known for its application in superconductor films and has been extensively studied in that context [50–53], its application as a strengthening agent in Ni-B composite coatings for tribological applications represents a novel and previously unexplored area. MgB_2 is a hard ionic compound [48,54,55], suggesting its potential use as a strengthening phase in the production of hard composite coatings. This research innovatively investigates the effects of MgB_2 particle incorporation at different concentrations (0.1, 0.25, and 0.5 g) on the structural, chemical, mechanical, tribological, wettability, and antibacterial properties of electroless Ni-B coatings deposited on AZ91 magnesium alloy substrates. By advancing our understanding of MgB_2's role in composite coatings, this study aims to contribute to the field of surface engineering, particularly in enhancing the performance and durability of coatings applied to magnesium alloys.

2. Experimental method

An AZ91 magnesium alloy containing approximately 9 % aluminum and 1 % zinc was the substrate material. By means of a lathe, cylindrical bars with a diameter of 20 mm were cut with a thickness of 5 mm and prepared for coating. The successful completion of the electroless coating depends on applying preliminary preparation processes to the substrate material before deposition. The adhesion of the coating to the substrate surface depends significantly on the cleanliness of the surface. The AZ91 magnesium alloy materials utilized in this investigation were initially rough-polished using 800 and 1200 grit sandpapers, followed by fine polishing with alumina powder. The substrates were immersed in acetone in an ultrasonic cleaner device for 5 min to remove any remaining dust and oil deposits. Following the mechanical polishing processes, pure water and prepared solutions were used for cleaning and activation processes. The initial step was to cleanse the surface of the samples from the oil layer by immersing them in an alkaline solution containing 50 g. L^{-1} NaOH +10 g. L^{-1} Na_3PO_4 at 60 °C for 6–10 min, followed by rinsing with pure water. Subsequently, they were immersed in a solution containing 125 g. L^{-1} CrO_3 + 110 mL. L^{-1} HNO_3 at room temperature for a duration of 4–6 s. After etching for a while, they were rinsed with distilled water and then soaked in an HF acid solution at room temperature for 3–5 s. After activating the sample surfaces, they were rinsed with alcohol and dried immediately with a hot fan.

The AZ91 magnesium alloy substrate materials were coated with two types of coatings: the Ni-B coating without MgB_2 reinforcement (as-deposited) and the Ni-B/MgB_2 composite coatings reinforced with MgB_2 in three different quantities. The selection of substances for the coating solutions and bath parameters was made based on considerations from the literature [56–64]. A 1-liter flask was used to prepare the Ni-B solution, which was then divided equally into 4 separate 250 ml flasks. Each flask was stirred using a magnetic stirrer with a stir bar for 30 min. Each of the solutions in the bottles was heated separately before the coating process, thoroughly mixed to ensure homogeneity, and prepared for deposition.

The SHIMADZU HMV-G20 microhardness measuring device was utilized to determine the microhardness values of the samples. Measurements were taken using the Vickers indenter tip with a 100 g load and a 10-s dwell time, acquiring measurements from five distinct points. A pin-on-disc wear test was conducted on the coated samples using a Bruker-UMT tribometer tester. As the counterpart, a 6 mm-diameter 316 austenitic stainless-steel ball was used. The samples underwent a dry sliding wear test with a sliding speed of 50 rpm and a constant load of 1 N. The means of friction coefficient values obtained from the pin-on-disc wear test represent the overall trend of friction coefficients. Surface roughness values were measured using a 3D profilometer device branded as Bruker Contour GT. The coated samples were analyzed using GNR-Explorer XRD device with a Cu-Kα (λ = 1.5405 A°) radiation source. The diffraction patterns were collected over an angular range of 10°–100° and with a step size of 0.1° per second. The acquired data were analyzed by comparing them to XRD spectra found in the literature and by using Match software. Using a Quanta-FEG 250 scanning electron microscope (SEM), both the substrate and coated samples were morphologically analyzed. Additionally, the wear marks obtained from the wear test were observed. The wettability of the samples was determined using an optical contact angle analyzer (KSV CAM-101). 6

Table 1
The composition of the coating solution and the conditions during the deposition process.

Bath conditions	Amount (g. L^{-1})
Nickel chloride ($NiCl_2$)	10
Sodium hydroxide (NaOH)	90
Ethylene diamine (NH_2-CH_2-CH_2-NH_2)	90
Lead nitrate (Pb^{+2}($PbNO_3$)	0.0145
Sodium borohydride ($NaBH_4$)	1.2
Bath temperature	90 °C
pH	13
Amount of MgB_2 reinforcing powder in 1000 mesh size	0.1, 0.25 and 0.5
Deposition time	60 min.

μL of distilled water was dispensed onto the samples, and the contact angle of the droplets with the surface was measured using a goniometer. The antimicrobial activity against *Escherichia coli* O157 (*E. coli*, gram-negative) was determined using the nutrient agar disc diffusion method. Bacterial suspensions containing 108 CFU mL^{-1} were transferred from bottles containing 25 mL of sterile nutrient agar to 9 cm Petri dishes. They were then spread evenly across the surface using a sterile stick, ensuring complete coverage of the Petri plate area. Thus, most of the bacteria were transferred to the culture medium that selectively supports the growth of anaerobes. The Petri dishes were incubated at 37 °C for 24 h, after which the zone diameters around the samples (inhibition zones) were measured using an optical microscope to evaluate the test results.

3. Result and discussion

Fig. 1 presents the comparative XRD spectra of the substrate and coated samples. From the XRD spectra, it is evident that the AZ91 substrate exhibits characteristic pronounced peaks corresponding to magnesium (100), (002), and (110) planes, along with weak peaks related to Al_2Mg (222). It is observed that as a result of Ni-B coating, nearly all peaks from the substrate are screened, and Ni-B (110) at 2θ ~ 33.09°, Ni-B (021) at 2θ ~ 39.01°, weak Ni_2B and Ni_3B phases between 2θ ~ 40°–50° is formed, as well as Ni-B (111) phase at 2θ ~ 45.46°. It is possible to infer that the Ni-B film is amorphous based on the low intensities of the crystalline peaks. Thus, the coating, which has not undergone heat treatment, indicated an incomplete crystallization process and contained a significant amount of Ni-B interstitial solid solution. It is observed that lower-intensity magnesium peaks, such as 2θ ≈ 32° (110), 34.3° (002), 36.7° (101), and 57.6° (110), appear at angles and planes similar to those found in the substrate when MgB_2 particles are added to the electroless Ni-B coating solution in varying amounts. The intensity of these peaks slightly increases with the increase in MgB_2 reinforcement. It is observed that the MgB_2 phase with the same crystal structure forms peaks at 2θ ~ 32° (110) and 2θ ~ 47.9° (002), indicating the Mg phase reflected from the substrate. Although the 2θ ~ 32° (110) and 2θ ~ 47.9° (002) plane reflections of magnesium from the substrate vanish with the as-deposited coating, it is notable that the intensity of these planes increases with higher amounts of reinforcement. This situation may be attributed to the crystal structure compatibility between magnesium and MgB_2. As reported in studies by Prikhna et al. [65–67], the synthesis of pure MgB_2 is practically impossible without oxygen. According to our observations, we confirmed the formation of the following phases: a $MgB_2O(OH)_6$ borate phase at 2θ ~ 16.4°, MgB_2O_5 at 2θ ~ 18.5°, MgO at 2θ ~ 44°, and the (013) $MgB_{2x}O_y$ oxide phases at 2θ ~ 63°. It was observed that the intensity of these oxide and borate phases decreased as the amount of reinforcement increased.

Fig. 2 shows the images of Ni-B coatings and AZ91 substrate. In Fig. 2a, it is evident that the etched AZ91 magnesium alloy used as the substrate contains the α (Mg) and β ($Mg_{17}Al_{12}$) phases, which are similar to the images obtained in the literature [68,69]. Fig. 2b illustrates a sample coated via electroless deposition with a thickness of 10 μm. The coatings exhibited a compact, dense, and uniform structure. No gaps were observed between the coating and the substrate, indicating a successful diffusion process under the specified conditions. This observation also attests to the robust bonding state achieved during the coating process, highlighting the effectiveness of the metallurgical connection between the coating and the substrate. The Ni-B coating has a typical cauliflower-like morphology [3,70,71] as shown in Fig. 2c. The obtained result is in line with the XRD analysis. Comparison of the XRD results indicates that the

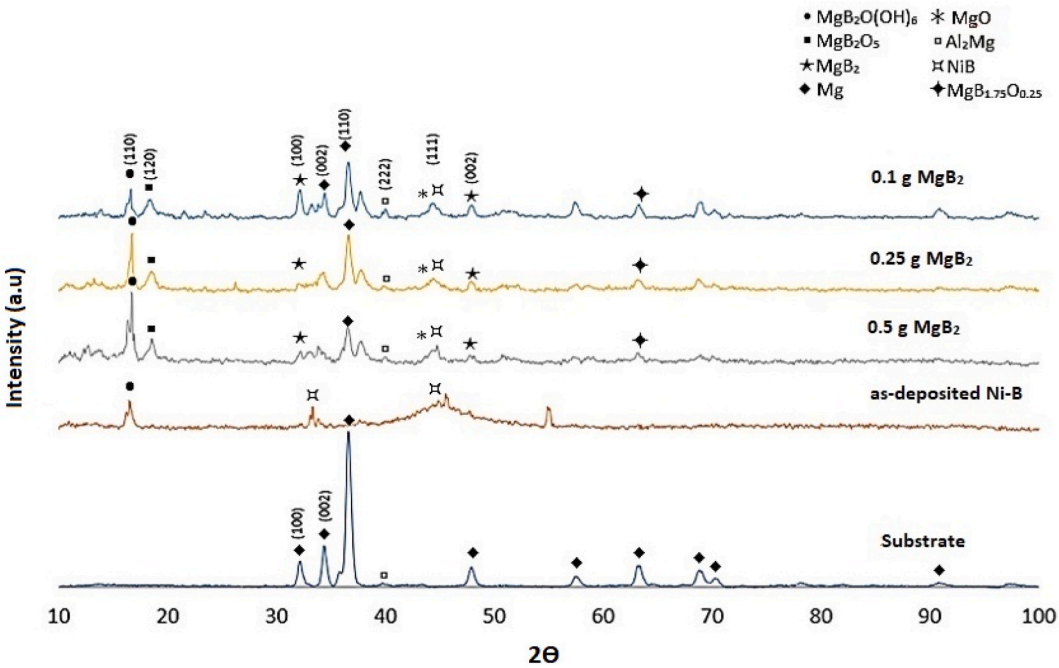

Fig. 1. XRD spectrum pattern of Ni-MgB_2 composite coatings at different MgB_2 particles amount.

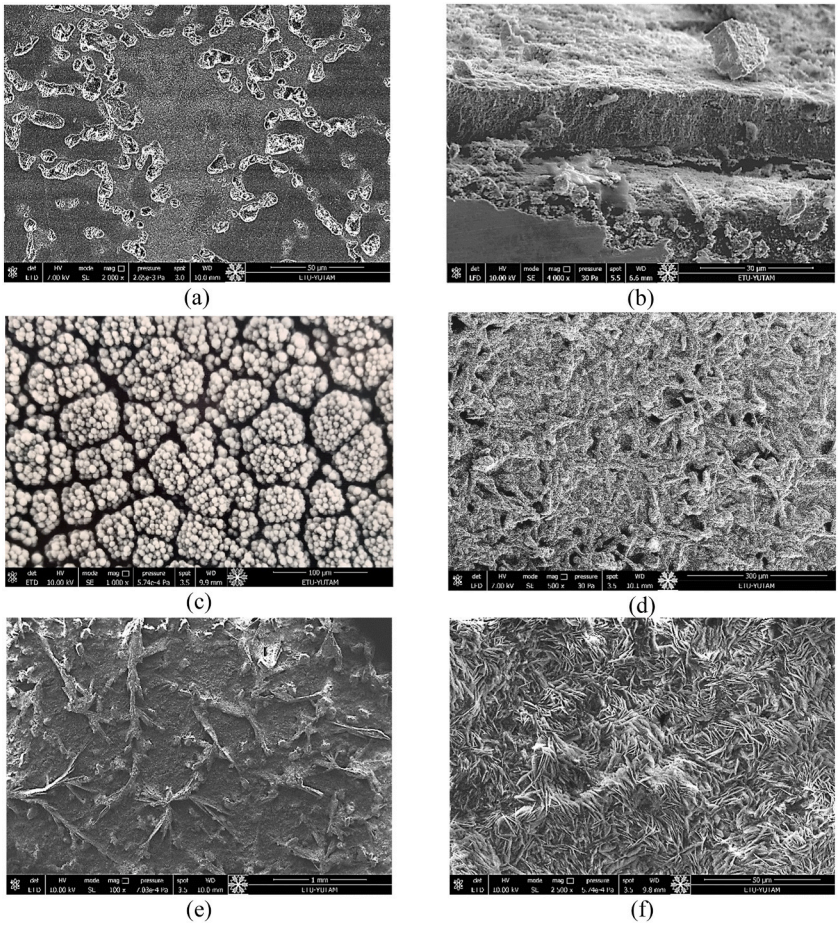

Fig. 2. SEM images of (a) substrate (b) typical cross-sectional interface (c) Ni-B coating (d) 0.1 g of MgB_2 reinforced Ni-B coating (e) 0.25 g of MgB_2 reinforced Ni-B coating (f) 0.5 g of MgB_2 reinforced Ni-B coating surfaces.

cauliflower-like structure of Ni-B diminishes with increasing incorporation of MgB_2. From Fig. 2d, it can be inferred that local spherical particles, dendrite-like [72] and irregular fibrous structures are formed as a result of local nucleation, which takes place at the cauliflower grain boundaries depending on the Mg, MgB_2, MgB_2O_5, MgO, $MgB_{2x}O_y$, and $MgB_2O(OH)_6$ phases obtained that result from a 0.1 g of MgB_2 incorporation. The Mg, MgB_2, MgB_2O_5, MgO, and $MgB_{2x}O_y$ phases developed and intensified, leading to more prominent intertwining and adhesion of MgB_2 ribbon structures with the Ni-B matrix with 0.25 g of MgB_2 reinforcement (Fig. 2e).

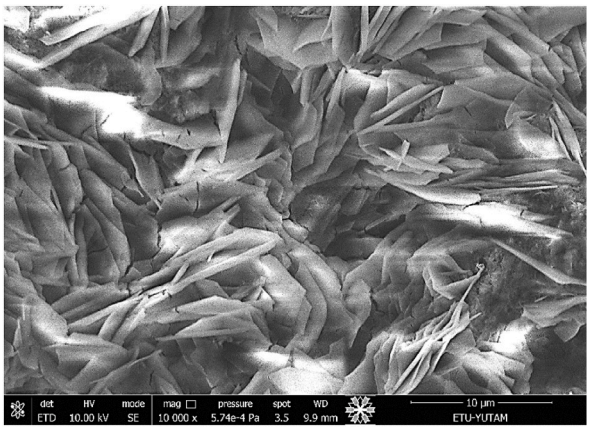

Fig. 3. Randomly oriented MgB_2 hexagonal sheets or platelets.

Furthermore, with the incorporation of 0.5 g of MgB_2, a granular structure with randomly oriented crystallites is observed to completely cover the Ni-B cauliflower-like structures, indicating the intensified presence of magnesium-based phases (Fig. 2f). This structure resembles to those observed in Refs. [73–76]and it is easier to understand this structure as platelet-like with a higher magnification SEM image of 10000× (Fig. 3). These platelet structures are attributed to MgB_2, as confirmed by XRD analyses. The platelets exhibit hexagonal crystallographic symmetry within a tightly packed hexagonal structure [77]. At the same time, this situation results in the material exhibiting anisotropic properties depending on the preferential orientation of the grains [78–81]. As a result, it can be concluded that the cauliflower-like Ni-B structure diminishes, and the level of precipitation of hexagonal MgB_2 crystals on the surface increases significantly, depending on the increase in the incorporation of MgB_2 in the deposition process.

In Fig. 4, the microhardness values of the substrate and the coated samples are presented. The Ni-B coating on AZ91 substrate material increased the hardness value, consistent with findings from previous studies [71,82,83]. The Ni-B deposition process increased it to 600 Vickers, compared to the substrate's hardness value of 80 Vickers. The hardness values of Ni-B/MgB_2 composite coatings produced with additions of 0.1 g, 0.25 g, and 0.5 g were 380 Vickers, 400 Vickers, and 490 Vickers, respectively. These obtained values are comparable to the hardness value of the electroless MgB_2 coating obtained on the AZ91 substrate before [48]. The microhardness values of the composite coatings were observed to be five or six times higher than the substrate's hardness, yet lower than that of the as-deposited Ni-B coating. Typically, materials with smaller grain sizes, such as Ni-B nanocrystalline deposits, are generally harder than materials with larger grain sizes. As the grain size decreases, the number of grain boundaries increases, which impedes the movement of dislocations and leads to an increase in hardness [84].

The friction coefficient-time relations of the samples are depicted in Fig. 5. The prepared Ni-B coating decreased the friction coefficient from approximately 0.22 to 0.16 and became more stable compared to the substrate. Although the addition of MgB2 reinforcement caused the coefficient of friction to increase approximately threefold, the friction coefficients decreased with higher amounts of reinforcement and exhibited greater stability when comparing MgB_2-reinforced coatings among themselves. The electroless MgB_2 coating on the AZ91 substrate is noted to reduce the friction coefficient of the coating layer by 40 % in a study [48]. This contrasting situation could be associated with the composite structure of the amorphous Ni-B matrix reinforced by MgB_2. Barati and Hadavi [85] attributed one reason for the increase in the friction coefficient to the uniform distribution of hard nanoparticles in the nanocomposite coating, thereby filling the pores in the coating. They suggested that this situation increases the resistance to sliding, and thereby causing an increase in the friction coefficient. The variations in average friction coefficient values observed for each of the MgB_2 reinforced composite coatings may be attributed to several factors. These include the dimensional, geometric, crystallographic, and morphological properties of MgB_2 particles, as well as their derivatives such as $MgB_2O(OH)_6$ and MgB_2O_5 hard particles. These particles are involved in the Ni-B interstitial solid solution, influencing the degree of their distribution within the coating.

The synergistic effect of these features caused fluctuations in friction values, resulting in the formation of a band pattern. Band formation in the coefficient of friction (COF) can occur due to various factors: adhesive interactions, surface roughness, wear debris accumulation, and chemical reactions. MgB_2 is a compound with a strong ionic bond between its atoms [86,87]. Additionally, MgB_2 compounds such as $MgB_2O(OH)_6$ (pinnoite) and MgB_2O_5 (pentoxide) are covalently bonded hard compounds. In the stick-slip mechanism [88–92] two surfaces dynamically interact causing fluctuating friction forces as they alternately adhere and slide against each other, thereby resulting in banding. Brink et al. [93] have expanded on this scenario by linking it to surface roughness, highlighting that both friction and wear volume increase with surface roughness. The graph in Fig. 7 demonstrates that the surface roughness increases with the increase in MgB_2 reinforcement. Thus, the abrasive wear resulting from the separation of MgB_2-based particles from the coating surface and their filling of the valleys created during sliding wear may be a cause of banding. They have also suggested that the friction behavior may change due to the heating and melting of the third body composed of wear particles and structures resulting from their agglomeration. Palaniappa and Seshadri [94] have also emphasized out that the $MgB_2O(OH)_6$ hard particles and MgB_2O_5 oxide phases play a crucial role in increasing wear. Furthermore, the preferential orientation of the hexagonal

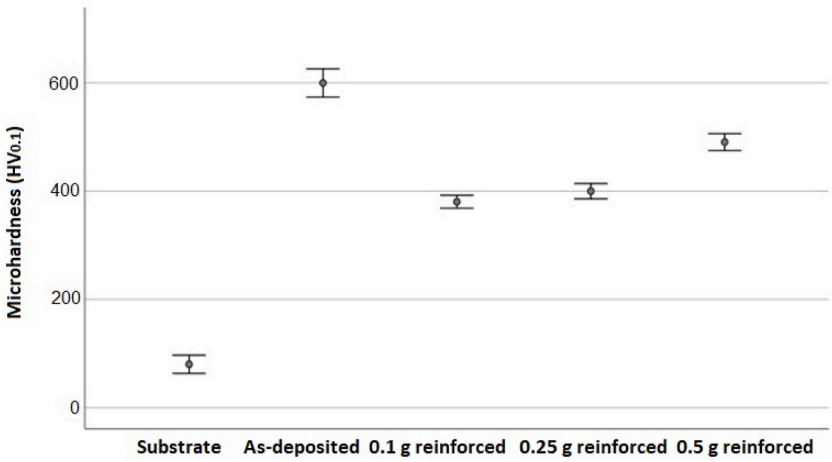

Fig. 4. Comparison of the microhardness values with error bars for samples.

Sample	Friction coefficient-time curves	Average friction coefficient (μ)
(a) Substrate	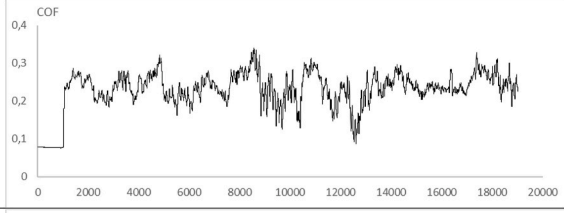	0.22
(b) Ni-B coating	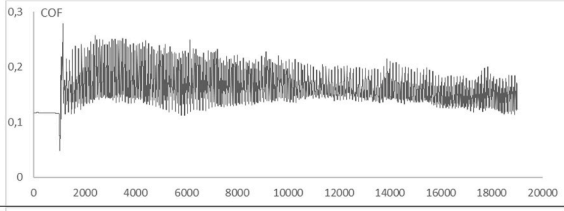	0.16
(c) 0.1 g of MgB_2 reinforced Ni-B coating	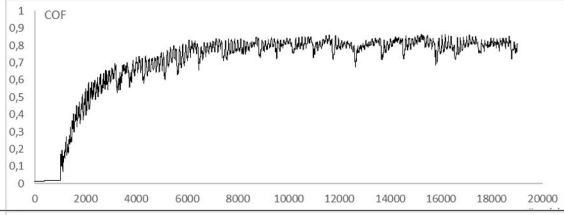	0.8
(d) 0.25 g of MgB_2 reinforced Ni-B coating	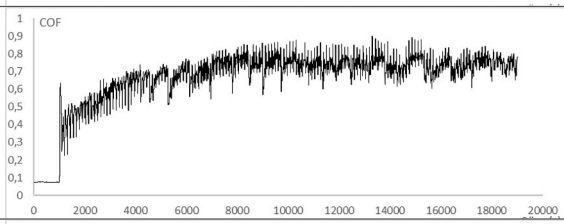	0.7
(e) 0.5 g of MgB_2 reinforced Ni-B coating	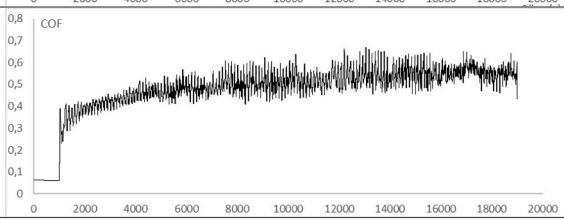	0.5

Fig. 5. Friction coefficient-time relationships of samples.

MgB_2 crystals in the direction of shear during wear may be responsible for the transition to a more stable and lower friction behavior brought about by the increase in MgB_2 reinforcement, as shown in Fig. 5e. This idea is also supported by the wear trace shown in Fig. 6e. SEM images of the samples after wear are given in Fig. 6. In the incorporated composite coatings, particularly those containing 0.25 g and 0.5 g of MgB_2 particles, wear debris was observed along the wear scar with coating material transferred around the wear track. This suggests the formation of a transfer film between the counterpart and the coating. The coating products dragged as a result of wear were plastered by being carried to the wear edges as a result of ploughing wear rather than a fragmented dispersed structure.

The oxide film that commonly forms on stainless steel contact surfaces at low loads prevents metallic bonding between mating materials, resulting in oxidative or mild wear characterized by a low wear rate. Kapoor and Johnson have observed that under low contact loads, the response can be predominantly elastic or lead to elastic shakedown [95]. However, under high loads, this oxide film breaks down, leading to severe wear characterized by rapid material loss and high wear-particle generation. Given the naturally occurring chromium oxide layer on stainless steel surfaces, which exhibits a hardness ranging from 2000 to 3000 HV, it is evident that this oxide is significantly harder than our produced coatings. Therefore, the probability of chromium oxide fracturing and causing abrasive effects during sliding is very low, even in scenarios where wear may cause particles to detach from the pin surface. This is because magnesium oxides within the worn coating on the opposing surface, along with chromium oxides, can create mechanically mixed hard layers or tribolayers on the contact surface, thereby mitigating abrasive effects and reducing wear [96]. Additionally, wear tests conducted at normal room temperature, low speeds, and loads ensure that high temperatures do not occur on worn component surfaces and that there is no increase in oxide layer thickness. Hence, the possibility of the oxide layer fracturing and causing abrasive

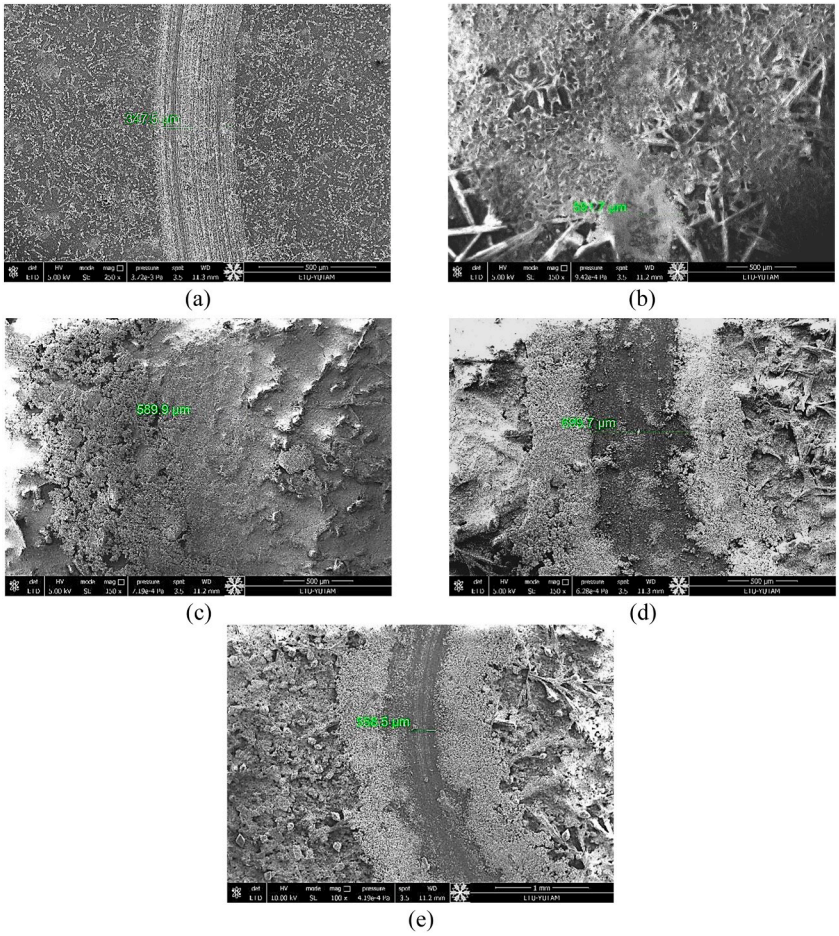

Fig. 6. SEM images of wear tracks: (a) substrate (b) Ni-B coating (c) 0.1 g of MgB_2 reinforced Ni-B coating (d) 0.25 g of MgB_2 reinforced Ni-B coating (e) 0.5 g of MgB_2 reinforced Ni-B coating.

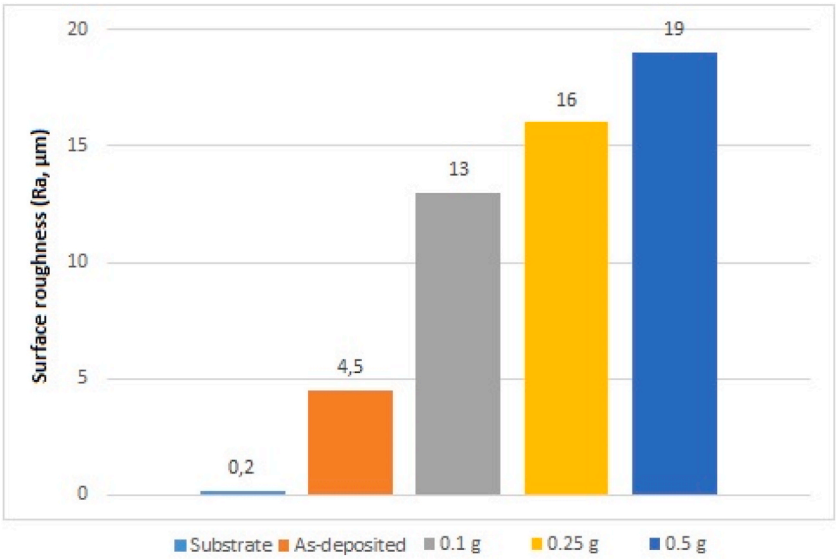

Fig. 7. Average surface roughness values of samples.

effects or fracture is minimal. As observed in Fig. 6a and d, the wear marks exhibit patterns indicative of ductile behavior. Consequently, the particle-reinforced composite coatings demonstrate a more stable wear curve compared to Ni-B coatings, as the worn samples show wear tracks extending to the edges without cracks and fractures that would indicate brittle failure within the wear track.

The average surface roughness values of the AZ91 magnesium alloy substrate, Ni-B coating, and MgB_2 reinforced composite coatings are depicted in Fig. 7 as a bar graph. The surface roughness value in the unreinforced coating is slightly higher due to the characteristic microstructure of Ni-B. In MgB_2 reinforced composite coatings, a significant increase in surface roughness value is observed. The reason for this increase is attributed to hexagonal MgB_2 particles entering the Ni-B matrix structure, where they serve as nucleation centers for the formation of larger grains. Comparing the composite coatings among themselves, the increase in reinforcement leads to localized agglomeration, which directly results in an increase in surface roughness (Fig. 8). A typical SEM image showing the localized agglomerations on the coating surface where the highest roughness value ($R_a = 19$ μm) is observed is provided in Fig. 8c.

The contact angles measured on the samples were utilized to assess their wettability characteristics. Fig. 9 illustrates the dispersion of water droplets on the samples, and the contact angles of the droplets with the surface are 98.28° (hydrophobic) for the substrate, 39.33° (hydrophilic) for Ni-B coating, and 32.40° (hydrophilic) for 0.1 g of MgB_2 reinforced Ni-B coating, respectively. Additionally, the Ni-B coating reinforced with 0.25 g of MgB_2 has a contact angle of 4.04° (superhydrophilic), while the coating reinforced with 0.5 g of MgB_2 has a contact angle of 23.6° (hydrophilic). The measured contact angles indicate that any coating type applied to the hydrophobic substrate material can result in the surface becoming a hydrophilic structure. MgB_2 reinforced coatings are more wettable than Ni-B coatings. The adhesion of MgB_2 and other derivatives with water, depending on their microstructural characteristics, and the increasing surface roughness are the reasons why increasing the amount of reinforcement decreases the contact angle. Previous studies in the literature corroborate that MgB_2 exhibits super hydrophilic properties [47,48]. Additionally, Wenzel [97,98] have declared the relationship between surface roughness and hydrophobicity.

The situation observed in the composite coatings produced in Fig. 10 is shown with the Wenzel model. In this manner, partial changes in hydrophilic properties depending on the amount of MgB_2 reinforcement are attributed to the factors such as the roughness levels, distributions, shapes, and distance between the roughness of the coatings, as described by the Wenzel model. According to the Wenzel model, when liquid molecules come into contact with a solid surface, they completely fill all the recesses, thereby increasing the surface's wettability as its roughness increases. Hydrophilic and superhydrophilic surfaces have the potential to be used in wastewater treatment, reclamation of ground and surface water, separation of liquid mixtures, biomedical applications, and places where self-cleaning, anti-fogging and corrosion resistance are required [99].

In Fig. 11, the antibacterial results of the substrate, as-deposited Ni-B coatings, and MgB_2 reinforced coatings are presented. The best antibacterial property among the coatings was obtained in the MgB_2 particle-reinforced coating with 0.1 g. The inhibition halo measurements show that MgB_2 particle-reinforced composite coatings exhibit greater antibacterial properties compared to Ni-B coatings. Consistent with the literature, it has been established that hydrophilic surfaces inhibit bacterial growth [100].

The medical field can profit from the use of a material imparted both hydrophilic and antibacterial qualities, particularly in prostheses and vascular inserts, as it can prevent bacterial adhesion and infection on the surface [101]. Additionally, it has been

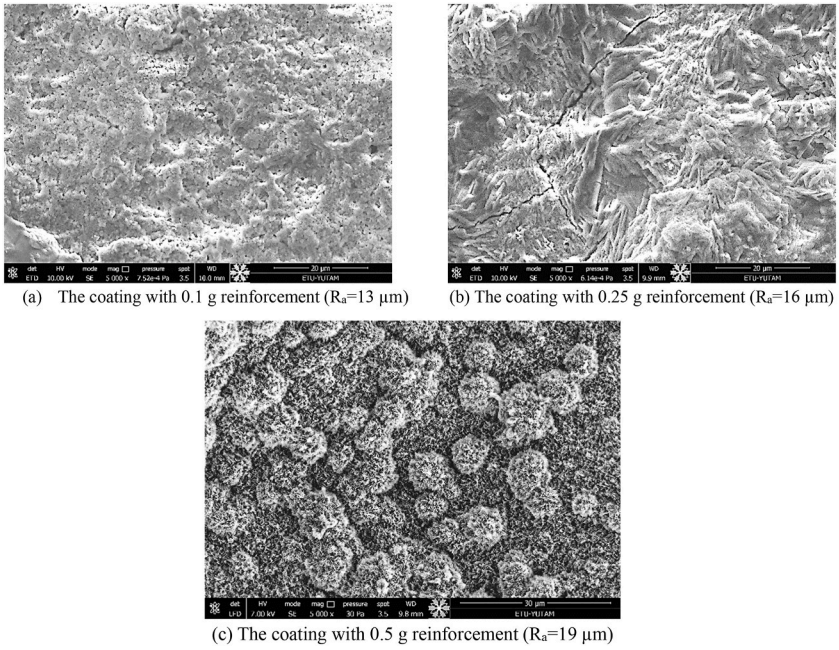

(a) The coating with 0.1 g reinforcement (R_a=13 μm) (b) The coating with 0.25 g reinforcement (R_a=16 μm)

(c) The coating with 0.5 g reinforcement (R_a=19 μm)

Fig. 8. Changes in surface structure and increasing surface roughness with increasing reinforcement amount (5000× magnification).

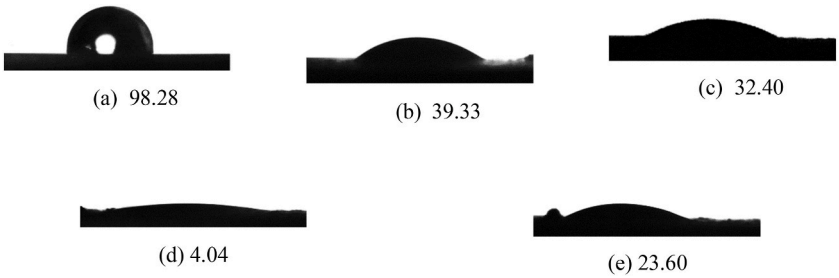

Fig. 9. Contact angles: (a) steel substrate (b) Ni-B coating (c) 0.1 g of MgB_2 reinforced Ni-B coating (d) 0.25 g of MgB_2 reinforced Ni-B coating (e) 0.5 g of MgB_2 reinforced Ni-B coating.

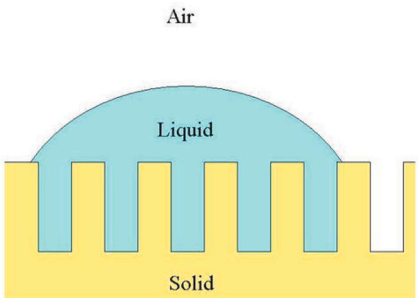

Fig. 10. Schematic representing of Wenzel model.

demonstrated that superhydrophilic membranes designed for water remediation reduce cohesion-free energy and possess qualities that inhibit biofilm formation and biopollution [99].

4. Conclusions

This study provided some insights into the structural, morphological, mechanical, tribological, antibacterial and contact angle properties induced by the electroless Ni-B coating process added MgB_2 particles on the AZ91 magnesium alloy substrate. The key findings and conclusions drawn from this research are summarized as follows:

Structural and Morphological Changes: X-ray diffraction (XRD) analysis revealed that the amorphous Ni-B coating effectively masked the magnesium peaks of the substrate, while MgB_2 incorporation led to the formation of $MgB_2O(OH)6$, MgB_2O_5, MgO, and $MgB_{2x}O_y$ oxide phases. Scanning electron microscopy (SEM) images showed that MgB_2 reinforcement altered the coating morphology from cauliflower-like Ni-B structures to dendritic and fibrous MgB_2 forms, progressing to granular structures with platelet-like MgB_2 crystals at higher concentrations.

Hardness Properties: Ni-B/MgB_2 coatings exhibited enhanced hardness compared to the substrate (80 HV), although lower than as-deposited Ni-B (600 HV). Microhardness values of composite coatings increased with MgB_2 reinforcement, indicating improved mechanical strength. The microhardness value of the coating reinforced with MgB_2 was 380 HV with 0.1 g of MgB_2, and it reached up to 490 HV with the addition of 0.5 g of MgB_2, demonstrating a significant improvement in mechanical properties.

Friction Properties: Initially, friction coefficient decreased with as-deposited Ni-B coating, increased significantly (threefold) with 0.1 g MgB_2, and then decreased and improved stability with higher reinforcement, although remaining higher than the as-deposited Ni-B coating. This behavior suggests a behavior complex interplay between MgB_2 particles, the Ni-B matrix, and counterpart affecting frictional and wear resistance. SEM analysis of wear tracks indicated transfer films and ploughing wear mechanisms influenced by MgB_2 particles.

Surface Roughness and Wettability: MgB_2 reinforcement increased surface roughness due to the formation of MgB_2 crystals, leading to localized agglomerations. This phenomenon significantly impacted wear characteristics, friction coefficients, and surface wettability. MgB_2-reinforced coatings exhibited varying hydrophilicity, with superhydrophilic properties observed at higher MgB_2 concentrations due to increased surface roughness and MgB_2's inherent properties.

Antibacterial Properties: MgB_2-reinforced composite coatings, particularly with 0.1 g MgB_2, demonstrated significantly improved antibacterial activity compared to the as-deposited Ni-B coating. The enhancement in inhibiting bacterial growth, attributed to the hydrophilic nature and structural features induced by MgB_2 particles.

Applications and Future Directions: The study highlights the potential of Ni-B/MgB_2 coatings for advanced surface engineering applications, particularly in industries requiring enhanced mechanical strength, wear resistance, hydrophilicity, and antibacterial properties (for example, biomedical and environmental applications). In conclusion, the study underscores MgB_2 as a promising

Sample	View	Zone diameter (mm)
Substrate	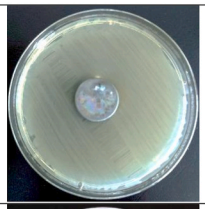	No zone
Ni-B coating		28
0.1 g of MgB_2 reinforced Ni-B coating	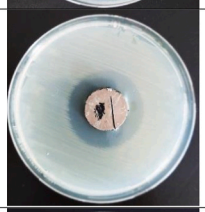	40
0.25 g of MgB_2 reinforced Ni-B coating	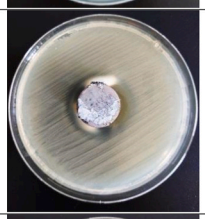	34
0.5 g of MgB_2 reinforced Ni-B coating		30

Fig. 11. Antibacterial test results of samples.

reinforcing agent in electroless Ni-B coatings, offering improvements in mechanical strength, frictional behavior, surface wettability, and antibacterial properties. Further optimization of MgB_2 concentration and deposition parameters could enhance these coatings' performance for advanced surface engineering applications on magnesium alloys.

The Ni-B/MgB_2 composite coatings, despite exhibiting higher hardness than the steel substrate, did not surpass the as-deposited Ni-B coating in terms of hardness and friction aspects. Non-optimal MgB_2 reinforcement amounts, deposition conditions, particle size, and phase incompatibility between MgB_2 and Ni-B may have been responsible for this result. Therefore, this outcome indicates the need for further research to identify ideal parameters. Furthermore, Stabilizers [46,102–110] are often used in nickel-boron coatings to manage challenges such as metal powder accumulation and instability, despite the use of complexing agents in plating baths. We did not explore the stabilizer's effect in this study; further research is needed to assess their suitability for manufacturing Ni-B/MgB_2 composite coatings. Theoretical and experimental studies are currently underway to improve the properties of alloys and coatings through applications or manufacturing processes involving solid solution, composites, and layered structures [111–115].

Data and code availability

Data will be aviable on request.

CRediT authorship contribution statement

Ferhat Bülbül: Writing – review & editing, Writing – original draft, Visualization, Validation, Supervision, Resources, Project administration, Methodology, Investigation, Funding acquisition, Formal analysis, Data curation, Conceptualization. **Tuğçenur Kılcı:**

Writing – original draft, Visualization, Investigation.

Declaration of competing interest

The authors declare that they have no known competing financial interests or personal relationships that could have appeared to influence the work reported in this paper.

Acknowledgement

This research is a part of Erzurum Technical University Research Funding BAP supported by grant no: 2021/005. The authors thank Erzurum Technical University for funding the project. In addition, they also thank lecturer Dr. Mustafa Yazıcı, for conducting the XRD, SEM, and tribological analyses, and Dr. L. Elif Bülbül for antibacterial tests. The authors would like to thank Assist. Prof. Dr. Kübra Güneş for her assistance with the static contact angle measurements.

References

[1] M. Hara, et al., Environmentally friendly composite film of anodizing and electrodeposition coating having a high corrosion resistance on magnesium alloy AZ91D, Mater. Trans. (2007), https://doi.org/10.2320/matertrans.MRA2006632.
[2] J. Tan, Ramakrishna S.Applications of magnesium and its alloys: A review, Applied Sciences 11 (15) (2021) 6861, https://doi.org/10.3390/app11156861.
[3] K. Krishnaveni, T.S.N. Sankara Narayanan, S.K. Seshadri, Electroless Ni–B coatings: preparation and evaluation of hardness and wear resistance, Surf. Coat. Technol. 190 (1) (Jan. 2005) 115–121, https://doi.org/10.1016/J.SURFCOAT.2004.01.038.
[4] V. Vitry, J. Hastir, A. Mégret, S. Yazdani, M. Yunacti, L. Bonin, "Recent advances in electroless nickel-boron coatings," (2022), https://doi.org/10.1016/j.surfcoat.2021.127937.
[5] T.C. Huang, M.C. Wei, H.I. Chen, Preparation of hydrogen-permselective palladium-silver alloy composite membranes by electroless co-deposition, Sep. Purif. Technol. 32 (1–3) (2003), https://doi.org/10.1016/S1383-5866(03)00063-7.
[6] S.C. Domenech, et al., Electroless plating of nickel-phosphorous on surface-modified poly(ethylene terephthalate) films, Appl. Surf. Sci. 220 (1–4) (2003), https://doi.org/10.1016/S0169-4332(03)00815-8.
[7] W.C. Wang, R.H. Vora, E.T. Kang, K.G. Neoh, Electroless plating of copper on fluorinated polyimide films modified by surface graft copolymerization with 1-vinylimidazole and 4-vinylpyridine, in: Polymer Engineering and Science, 2004, https://doi.org/10.1002/pen.20033.
[8] J. Sudagar, J. Lian, W. Sha, "Electroless nickel, alloy, composite and nano coatings - A critical review," (2013), https://doi.org/10.1016/j.jallcom.2013.03.107.
[9] I. Rajagopal, Electroless and electrodeposition of nickel boron composites, Bull. Mater. Sci. 5 (3–4) (1983), https://doi.org/10.1007/BF02744046.
[10] D. Dong, X.H. Chen, W.T. Xiao, G.B. Yang, P.Y. Zhang, Preparation and properties of electroless Ni-P-SiO 2 composite coatings, Appl. Surf. Sci. 255 (15) (2009), https://doi.org/10.1016/j.apsusc.2009.03.039.
[11] S. Sadreddini, A. Afshar, The effect of heat treatment on properties of Ni–P–SiO2 nano-composite coating, Protect. Met. Phys. Chem. Surface 52 (3) (2016), https://doi.org/10.1134/S2070205116030254.
[12] S. Sadreddini, A. Afshar, M.A. Jazani, Tribological properties of Ni–P–SiO2 nanocomposite coating on aluminum, Colloid J. 77 (5) (2015), https://doi.org/10.1134/S1061933X15050166.
[13] S. Rahemi Ardakani, A. Afshar, S. Sadreddini, A.A. Ghanbari, Characterization of Ni-P-SiO2-Al2O3 nano-composite coatings on aluminum substrate, Mater. Chem. Phys. 189 (2017), https://doi.org/10.1016/j.matchemphys.2016.12.023.
[14] D. Ekmekci, F. Bülbül, Preparation and characterization of electroless Ni-B/nano-SiO2, Al2O3, TiO2 and CuO composite coatings, Bull. Mater. Sci. 38 (3) (2015), https://doi.org/10.1007/s12034-015-0912-1.
[15] M. Matsuoka, T. Hotta, T. Tamura, T. Hayashi, Preparation of Ni-B-SiC composite coatings by electroless plating, J. Surf. Finish. Soc. Jpn. 40 (7) (1989), https://doi.org/10.4139/sfj.40.831.
[16] V. Nemane, S. Chatterjee, Evaluation of microstructural, mechanical, and tribological characteristics of Ni-B-W-SiC electroless composite coatings involving multi-pass scratch test, Mater. Char. 180 (2021), https://doi.org/10.1016/j.matchar.2021.111414.
[17] E. Georgiza, V. Gouda, P. Vassiliou, Production and properties of composite electroless Ni-B-SiC coatings, Surf. Coat. Technol. 325 (2017), https://doi.org/10.1016/j.surfcoat.2017.06.019.
[18] S. Zhang, K. Han, L. Cheng, The effect of SiC particles added in electroless Ni-P plating solution on the properties of composite coatings, Surf. Coat. Technol. 202 (12) (Mar. 2008) 2807–2812, https://doi.org/10.1016/j.surfcoat.2007.10.015.
[19] G. Jiaqiang, L. Lei, W. Yating, S. Bin, H. Wenbin, Electroless Ni-P-SiC composite coatings with superfine particles, Surf. Coat. Technol. 200 (20–21) (2006), https://doi.org/10.1016/j.surfcoat.2005.08.134.
[20] S.J. Yu, L.X. Song, Y.S. Huang, R.G. Zhao, X.F. Hu, Electroless Ni-P-SiC composite coating, Wuji Cailiao Xuebao/Journal of Inorganic Materials 19 (3) (May 2004) 647–652.
[21] J.P. Deepa, T.P.D. Rajan, C. Pavithran, B.C. Pai, Studies on electroless nickel boride coating on boron carbide particles, Surf. Eng. 30 (10) (2014), https://doi.org/10.1179/1743294414Y.0000000279.
[22] J.P. Ge, R.X. Che, X.Z. Wang, Structure & properties of electroless Ni-P-B 4C composite coatings, Plat. Surf. Finish. 85 (10) (1998).
[23] M. Rezagholizadeh, M. Ghaderi, A. Heidary, S.M. Monirvaghefi, The effect of B4C nanoparticles on the corrosion and tribological behavior of electroless Ni-B-B4C composite coatings, Surf. Eng. Appl. Electrochem. 51 (1) (2015), https://doi.org/10.3103/S1068375515010135.
[24] S.M. Monir Vaghefi, A. Saatchi, M. Ebrahimian-Hoseinabadi, Deposition and properties of electroless Ni-P-B4C composite coatings, Surf. Coat. Technol. 168 (2–3) (2003), https://doi.org/10.1016/S0257-8972(02)00926-X.
[25] M. Ebrahimian-Hosseinabadi, K. Azari-Dorcheh, S.M.M. Vaghefi, Wear behavior of electroless Ni-P-B4C composite coatings, Wear 260 (1–2) (2006), https://doi.org/10.1016/j.wear.2005.01.020.
[26] D.R. Dhakal, G. Gyawali, Y.K. Kshetri, J.H. Choi, S.W. Lee, Microstructural and electrochemical corrosion properties of electroless Ni-P-TaC composite coating, Surf. Coat. Technol. 381 (2020), https://doi.org/10.1016/j.surfcoat.2019.125135.
[27] M. Czagány, P. Baumli, Effect of surfactants on the behavior of the Ni-P bath and on the formation of electroless Ni-P-TiC composite coatings, Surf. Coat. Technol. 361 (2019), https://doi.org/10.1016/j.surfcoat.2019.01.046.
[28] A. Mazurek, G. Cieślak, W. Bartoszek, M. Trzaska, Abrasion resistance of Ni-B/Si3N4 composite layers produced by electroless method, Archives of Materials Science and Engineering 87 (1) (2017), https://doi.org/10.5604/01.3001.0010.5967.
[29] K. Krishnaveni, T.S.N.S. Narayanan, S.K. Seshadri, Corrosion resistance of electrodeposited Ni-B and Ni-B-Si3N4 composite coatings, J. Alloys Compd. 480 (2) (2009), https://doi.org/10.1016/j.jallcom.2009.02.053.
[30] K. Krishnaveni, T.S.N. Sankara Narayanan, S.K. Seshadri, Electroless Ni-B-Si 3N 4 composite coating: deposition and evaluation of its characteristic properties, Synth. React. Inorg. Metal-Org. Nano-Metal Chem. 42 (7) (2012), https://doi.org/10.1080/15533174.2011.618475.
[31] J.N. Balaraju, V. Ezhil Selvi, K.S. Rajam, Electrochemical behavior of low phosphorus electroless Ni-P-Si3N4 composite coatings, Mater. Chem. Phys. 120 (2–3) (2010), https://doi.org/10.1016/j.matchemphys.2009.11.047.

[32] A.A. Zuleta, et al., Preparation and characterization of electroless Ni-P-Fe3O4 composite coatings and evaluation of its high temperature oxidation behaviour, Surf. Coat. Technol. 203 (23) (2009), https://doi.org/10.1016/j.surfcoat.2009.05.025.

[33] V.B. Chintada, R. Koona, Preparation and properties of composite electroless Ni-P-ZnO coatings, Mater. Res. Innovat. 24 (2) (2020), https://doi.org/10.1080/14328917.2019.1582740.

[34] C. Feng, S. Hu, Y. Jiang, Y. Zhou, Effects of micro-arc oxidation of Ti6Al4V alloy on adhesion property to electroless Ni-P-ZrO2 composite platings and their wear resistance, Xiyou Jinshu Cailiao Yu Gongcheng/Rare Metal Materials and Engineering 42 (12) (2013) 2427–2432, https://doi.org/10.1016/s1875-5372(14)60032-1.

[35] W. Chen, W. Gao, Y. He, A novel electroless plating of Ni-P-TiO2 nano-composite coatings, Surf. Coat. Technol. 204 (15) (2010), https://doi.org/10.1016/j.surfcoat.2010.01.032.

[36] J. Novakovic, P. Vassiliou, K. Samara, T. Argyropoulos, Electroless NiP-TiO2 composite coatings: their production and properties, Surf. Coat. Technol. 201 (3–4) (2006), https://doi.org/10.1016/j.surfcoat.2006.01.005.

[37] X. Hu, S. Xu, Y. Yang, Z. Chen, Y.C. Chan, Effect of TiO2 nanoparticle addition on electroless Ni-P under bump metallization for lead-free solder interconnection, Mater. Sci. Eng. 600 (2014), https://doi.org/10.1016/j.msea.2014.02.011.

[38] X. Shu, Y. Wang, C. Liu, W. Gao, Microstructure and properties of Ni-B-TiO2 nano-composite coatings fabricated by electroless plating, Mater. Technol. 30 (A1) (2015), https://doi.org/10.1179/1753555714Y.0000000190.

[39] V. Niksefat, M. Ghorbani, Mechanical and electrochemical properties of ultrasonic-assisted electroless deposition of Ni-B-TiO2 composite coatings, J. Alloys Compd. 633 (2015), https://doi.org/10.1016/j.jallcom.2015.01.250.

[40] G. Cieślak, Corrosion properties of Ni-B/Al2O3 composites layers produced by electroless method, OCHRONA PRZED KOROZJĄ 1 (7) (2017), https://doi.org/10.15199/40.2017.7.1.

[41] M. Ghaderi, M. Rezagholizadeh, A. Heidary, S.M. Monirvaghefi, The effect of Al2O3 nanoparticles on tribological and corrosion behavior of electroless Ni–B–Al2O3 composite coating, Protect. Met. Phys. Chem. Surface 52 (5) (2016), https://doi.org/10.1134/S2070205116050087.

[42] J.N. Balaraju, Kalavati, K.S. Rajam, Influence of particle size on the microstructure, hardness and corrosion resistance of electroless Ni-P-Al2O3 composite coatings, Surf. Coat. Technol. 200 (12–13) (2006), https://doi.org/10.1016/j.surfcoat.2005.03.007.

[43] Y. de Hazan, D. Werner, M. Z'graggen, M. Groteklaes, T. Graule, Homogeneous Ni-P/Al2O3 nanocomposite coatings from stable dispersions in electroless nickel baths, J. Colloid Interface Sci. 328 (1) (2008), https://doi.org/10.1016/j.jcis.2008.08.033.

[44] D. Gultekin, E. Duru, H. Akbulut, Effect of heat treatment and applied load on mechanical and tribological properties of Ni-B-CeO2 composite electroless coating, European Journal of Science and Technology (2022), https://doi.org/10.31590/ejosat.1083546.

[45] J.K. Pancrecious, J.P. Deepa, V. Jayan, U.S. Bill, T.P.D. Rajan, B.C. Pai, Nanoceria induced grain refinement in electroless Ni-B-CeO2 composite coating for enhanced wear and corrosion resistance of Aluminium alloy, Surf. Coat. Technol. 356 (2018), https://doi.org/10.1016/j.surfcoat.2018.09.046.

[46] D. Gültekin, E. Duru, H. Akbulut, Improved wear behaviors of lead-free electroless Ni[sbnd]B and Ni-B/CeO2 composite coatings, Surf. Coat. Technol. 422 (2021), https://doi.org/10.1016/j.surfcoat.2021.127525.

[47] F. Bülbül, S. Jafarpour, M. Ertuğrul, The preparation of hard and super-hydrophilic MgB2 coating by spray pyrolysis deposition: Die Herstellung einer harten und superhydrophilen Magnesiumborid-Beschichtung (MgB2) durch Sprühpyrolyse Abscheidung, Mater. Werkst. 47 (9) (2016), https://doi.org/10.1002/mawe.201600454.

[48] F. Bülbül, M. Güney, S. Jafarpour, The synthesis of super-hydrophilic and hard MgB_2 coatings as an alternative to electroless nickel coatings, Kovove Mater. 56 (4) (2018), https://doi.org/10.4149/km_2018_4_223.

[49] K.S. Vijayaragavan, S.K. Putatunda, A. Dixit, G. Lawes, Electroless deposition of superconducting MgB2 films on various substrates, Thin Solid Films 519 (2) (2010), https://doi.org/10.1016/j.tsf.2010.08.107.

[50] M. Ranot, P.V. Duong, A. Bhardwaj, W.N. Kang, A review on the understanding and fabrication advancement of MgB2 thin and thick films by HPCVD, Progress in Superconductivity and Cryogenics (PSAC) 17 (2) (2015), https://doi.org/10.9714/psac.2015.17.2.001.

[51] J. Akimitsu, S. Akutagawa, K. Kawashima, T. Muranaka, Superconductivity in MgB2 and its related materials, Prog. Theor. Phys. Suppl. (2005), https://doi.org/10.1143/PTPS.159.326.

[52] M. Rafieazad, Ö. Balcı, S. Acar, M. Somer, Review on magnesium diboride (MgB2) as excellent superconductor: effects of the production techniques on the superconducting properties, Journal of Boron 2 (2) (2017).

[53] C. Buzea, T. Yamashita, "Review of the superconducting properties of MgB2," (2001), https://doi.org/10.1088/0953-2048/14/11/201.

[54] F. Karaboğa, Effect of rapidly annealing process on MgB2 superconducting wires, Sakarya University Journal of Science 23 (5) (2019), https://doi.org/10.16984/saufenbilder.552659.

[55] S.F. Matar, Electronic structure and chemical bonding within MgB2 and related borides from first principles, Zeitschrift fur Naturforschung - Section B Journal of Chemical Sciences 63 (6) (2008), https://doi.org/10.1515/znb-2008-0613.

[56] F. Bulbul, The effects of deposition parameters on surface morphology and crystallographic orientation of electroless Ni-B coatings, Met. Mater. Int. 17 (1) (2011), https://doi.org/10.1007/s12540-011-0210-4.

[57] F. Bülbül, Antibacterial activity of electroless Ni-B coating, Mater. Sci. Technol. 27 (10) (2011), https://doi.org/10.1179/1743284710Y.0000000042.

[58] F. Bülbül, H. Altun, O. Küçük, V. Ezirmik, Tribological and corrosion behaviour of electroless Ni-B coating possessing a blackberry like structure, Met. Mater. Int. 18 (4) (2012), https://doi.org/10.1007/s12540-012-4011-1.

[59] R. Sadeler, S. Çorak, S. Atasoy, F. Bülbül, Evaluation of an electroless nickel-boron (Ni-B) coating on corrosion fatigue performance of ball burnished AISI 1045 steel, Kovove Mater. 51 (6) (2013), https://doi.org/10.4149/km_2013_6_351.

[60] F. Bülbül, H. Altun, V. Ezirmik, O. Küçük, Investigation of structural, tribological and corrosion properties of electroless Ni-B coating deposited on 316L stainless steel, Proc. IME J. J. Eng. Tribol. 227 (6) (2013), https://doi.org/10.1177/1350650112464928.

[61] F. Bülbül, I. Çelik, Effect of heat treatment on structure of electroless Ni-B coated pure titanium, Journal of the Faculty of Engineering and Architecture of Gazi University 29 (1) (2014), https://doi.org/10.17341/gummfd.69914.

[62] I. Çelik, M. Karakan, F. Bülbül, Investigation of structural and tribological properties of electroless Ni-B coated pure titanium, Proc. IME J. J. Eng. Tribol. 230 (1) (2016), https://doi.org/10.1177/1350650115588568.

[63] F. Bülbül, L.E. Bülbül, Fabrication of antibacterial and hydrophilic electroless Ni–B coating on 316L stainless steel, Appl. Phys. Mater. Sci. Process 122 (1) (2016), https://doi.org/10.1007/s00339-015-9549-6.

[64] F. Bülbül, F. Karabudak, R. Yesildal, Production of hard hydrophilic Ni-B coatings on hydrophobic Ni-Ti and Ti-6Al-4V alloys by electroless deposition, Materialpruefung/Materials Testing 59 (6) (2017), https://doi.org/10.3139/120.111033.

[65] T.A. Prikhna, et al., Structure and properties of MgB2: effect of Ti-O and TiC additions, IEEE Trans. Appl. Supercond. 28 (4) (2018), https://doi.org/10.1109/TASC.2018.2794145.

[66] T.A. Prikhna, et al., Influence of oxygen concentration and distribution on microstructure and superconducting characteristics of MgB2-based materials and melt-textured YBCO, IEEE Trans. Appl. Supercond. 32 (4) (2022), https://doi.org/10.1109/TASC.2021.3139258.

[67] T.A. Prikhna, et al., Preparation and properties of MgB2 thin films, IEEE Trans. Appl. Supercond. 28 (7) (2018), https://doi.org/10.1109/TASC.2018.2844357.

[68] M. Thirumurugan, S. Kumaran, Extrusion and precipitation hardening behavior of AZ91 magnesium alloy, Trans. Nonferrous Metals Soc. China 23 (6) (2013), https://doi.org/10.1016/S1003-6326(13)62636-9.

[69] F. Aydin, R. Durgut, Estimation of wear performance of AZ91 alloy under dry sliding conditions using machine learning methods, Trans. Nonferrous Metals Soc. China 31 (1) (2021), https://doi.org/10.1016/S1003-6326(20)65482-6.

[70] M. Anik, E. Körpe, E. Şen, Effect of coating bath composition on the properties of electroless nickel-boron films, Surf. Coat. Technol. 202 (9) (2008), https://doi.org/10.1016/j.surfcoat.2007.07.031.

[71] F. Bülbül, Ni-B coating production on magnesium alloy by electroless deposition, Open 9 (6) (2015).

[72] T.P. Krinitsina, E.I. Kuznetsova, M.V. Degtyarev, Y.V. Blinova, "MgB2-Based Superconductors: Structure and Properties," (2021), https://doi.org/10.1134/S0031918X2112005X.
[73] V. Ferrando, et al., High upper critical field and irreversibility field in MgB 2 coated-conductor fibers, Appl. Phys. Lett. 87 (25) (2005), https://doi.org/10.1063/1.2149289.
[74] G.Z. Li, M.D. Sumption, E.W. Collings, Kinetic analysis of MgB2 layer formation in advanced internal magnesium infiltration (AIMI) processed MgB2 wires, Acta Mater. 96 (2015), https://doi.org/10.1016/j.actamat.2015.06.013.
[75] M. Maeda, et al., Interfacial reaction and side effect of MgB2 superconducting material through low-rotation mechanical milling, Ceram. Int. 48 (5) (2022), https://doi.org/10.1016/j.ceramint.2021.11.201.
[76] M. Paranthaman, et al., Superconducting MgB2 films via precursor postprocessing approach, Appl. Phys. Lett. 78 (23) (2001), https://doi.org/10.1063/1.1377323.
[77] U. Kölemen, Analysis of ISE in microhardness measurements of bulk MgB2 superconductors using different models, J. Alloys Compd. 425 (1–2) (2006), https://doi.org/10.1016/j.jallcom.2006.01.075.
[78] R. Flükiger, H.L. Suo, N. Musolino, C. Beneduce, P. Toulemonde, P. Lezza, "Erratum: superconducting properties of MgB2 tapes and wires, Physica C 385 (286–305) (2003) 2003, https://doi.org/10.1016/S0921-4534(03)00886-4. PII: S0921453402023079).
[79] N. Kaya, Ş. Çavdar, H. Koralay, Investigation of the effect of temperature on the structural and magnetic properties of MgB2 superconductor produced using boron doped with carbon by CVD method, Gazi Univ. fen Bilim. Derg. Part C: Tasarım ve Teknoloji 9 (2) (2021), https://doi.org/10.29109/gujsc.887430.
[80] N. Kaya, S. Cavdar, O. Ozturk, G. Yildirim, H. Koralay, Evaluation of superconducting features and gap coefficients for electron–phonon couplings properties of MgB2 with multi-walled carbon nanotube addition, J. Mater. Sci. Mater. Electron. 33 (7) (2022), https://doi.org/10.1007/s10854-021-07570-2.
[81] N. Kaya, Ş. Çavdar, Ö. Öztürk, H. Ada, H. Koralay, Investigation of microhardness properties of the multi-walled carbon nanotube additive MgB2 structure by using the vickers method, Cryogenics 116 (2021), https://doi.org/10.1016/j.cryogenics.2021.103295.
[82] E. Correa, et al., Nickel-boron plating on magnesium and AZ91D alloy by a chromium-free electroless process, Surf. Coat. Technol. 206 (13) (2012), https://doi.org/10.1016/j.surfcoat.2011.12.023.
[83] E. Correa, et al., Tribological behavior of electroless Ni-B coatings on magnesium and AZ91D alloy, Wear 305 (1–2) (2013), https://doi.org/10.1016/j.wear.2013.06.004.
[84] J. Novakovic, P. Vassiliou, Vacuum thermal treated electroless NiP-TiO2 composite coatings, Electrochim. Acta 54 (9) (2009), https://doi.org/10.1016/j.electacta.2008.12.015.
[85] Q. Barati, S.M.M. Hadavi, "Electroless Ni-B and composite coatings: a critical review on formation mechanism, properties, applications and future trends (2020), https://doi.org/10.1016/j.surfin.2020.100702.
[86] C.E. Kim, K.G. Ray, D.F. Bahr, V. Lordi, Electronic structure and surface properties of MgB2 (0001) upon oxygen adsorption, Phys. Rev. B 97 (19) (2018), https://doi.org/10.1103/PhysRevB.97.195416.
[87] P. De la Mora, M. Castro, G. Tavizon, Comparative study of the electronic structure of alkaline-earth borides (MeB2; Me = Mg, Al, Zr, Nb, and Ta) and their normal-state conductivity, J. Solid State Chem. 169 (2) (2002), https://doi.org/10.1016/S0022-4596(02)00045-2.
[88] R.P. Nachane, G.F.S. Hussain, K.R. Krishna Iyer, Theory of stick-slip effect in friction, Indian J. Fibre Text. Res. 23 (4) (1998).
[89] D. Perez, Y. Dong, A. Martini, A.F. Voter, Rate theory description of atomic stick-slip friction, Phys. Rev. B Condens. Matter 81 (24) (2010), https://doi.org/10.1103/PhysRevB.81.245415.
[90] M.E.R. Shanahan, Simple theory of 'stick-slip' wetting hysteresis, Langmuir 11 (3) (1995), https://doi.org/10.1021/la00003a057.
[91] L.M. Babici, A. Tudor, J. Romeu, Stick-slip phenomena and acoustic emission in the hertzian linear contact, Appl. Sci. 12 (19) (2022), https://doi.org/10.3390/app12199527.
[92] J. Awrejcewicz, P. Olejnik, Occurrence of stick-slip phenomenon, J. Theor. Appl. Mech. 45 (1) (2007).
[93] T. Brink, E. Milanese, J.F. Molinari, Effect of wear particles and roughness on nanoscale friction, Phys. Rev. Mater. 6 (1) (2022), https://doi.org/10.1103/PhysRevMaterials.6.013606.
[94] M. Palaniappa, S.K. Seshadri, Friction and wear behavior of electroless Ni-P and Ni-W-P alloy coatings, Wear 265 (5–6) (2008), https://doi.org/10.1016/j.wear.2008.01.002.
[95] A. Kapoor, A re-evaluation of the life to rupture of ductile metals by cyclic plastic strain, Fatig. Fract. Eng. Mater. Struct. 17 (2) (1994), https://doi.org/10.1111/j.1460-2695.1994.tb00801.x.
[96] M. Varga, H. Rojacz, H. Winkelmann, H. Mayer, E. Badisch, Wear reducing effects and temperature dependence of tribolayer formation in harsh environment, Tribol. Int. (2013), https://doi.org/10.1016/j.triboint.2013.03.003.
[97] R.N. Wenzel, Theory of wetting action at solid surfaces, Ind. Eng. Chem. 28 (8) (1936).
[98] Robert N. Wenzel, Resistance of solid surfaces to wetting by water, Ind. Eng. Chem. 28 (4) (1936).
[99] T.A. Otitoju, A.L. Ahmad, B.S. Ooi, "Superhydrophilic (superwetting) surfaces: A review on fabrication and application," (2017), https://doi.org/10.1016/j.jiec.2016.12.016.
[100] H. Qian, et al., Mussel-inspired superhydrophilic surface with enhanced antimicrobial properties under immersed and atmospheric conditions, Appl. Surf. Sci. 465 (2019), https://doi.org/10.1016/j.apsusc.2018.09.173.
[101] L. Li, et al., Nanoparticles-stacked superhydrophilic coating supported synergistic antimicrobial ability for enhanced wound healing, Biomater. Adv. 132 (2022), https://doi.org/10.1016/j.msec.2021.112535.
[102] L. Bonin, C.C. Castro, V. Vitry, A.L. Hantson, F. Delaunois, Optimization of electroless NiB deposition without stabilizer, based on surface roughness and plating rate, J. Alloys Compd. 767 (2018), https://doi.org/10.1016/j.jallcom.2018.06.330.
[103] L. Bonin, V. Vitry, F. Delaunois, Replacement of Lead stabilizer in electroless Nickel-Boron baths: synthesis and characterization of coatings from bismuth stabilized bath, Sustainable Materials and Technologies 23 (2020), https://doi.org/10.1016/j.susmat.2019.e00130.
[104] L. Bonin, V. Vitry, F. Delaunois, The tin stabilization effect on the microstructure, corrosion and wear resistance of electroless NiB coatings, Surf. Coat. Technol. 357 (2019), https://doi.org/10.1016/j.surfcoat.2018.10.011.
[105] S. Yazdani, V. Vitry, RSM models approach for optimization of the mechanical properties of electroless Ni-B-nanodiamond coating: an experimental and molecular dynamic simulation study, Surf. Coat. Technol. 452 (2023), https://doi.org/10.1016/j.surfcoat.2022.129133.
[106] A. Mukhopadhyay, T.K. Barman, P. Sahoo, Effect of heat treatment on microstructure and corrosion resistance of Ni-B-W-Mo coating deposited by electroless method, Surf. Rev. Lett. 25 (8) (2018), https://doi.org/10.1142/S0218625X19500239.
[107] R. Agrawal, A. Mukhopadhyay, Inclusion of W in electroless Ni–B coating developed from a stabilizer free bath and investigation of its tribological behaviour, J. Indian Chem. Soc. 100 (4) (2023), https://doi.org/10.1016/j.jics.2023.100966.
[108] R. Agrawal, A. Mukhopadhyay, Development of Ni-B electroless coating from stabilizer free bath and characterization of high temperature tribological behaviour, scratch and corrosion resistance, Surf Topogr 10 (4) (2022), https://doi.org/10.1088/2051-672X/aca784.
[109] T.S.N. Sankara Narayanan, S.K. Seshadri, Formation and characterization of borohydride reduced electroless nickel deposits, J. Alloys Compd. 365 (1–2) (2004), https://doi.org/10.1016/S0925-8388(03)00680-7.
[110] F. Delaunois, P. Lienard, Heat treatments for electroless nickel-boron plating on aluminium alloys, Surf. Coat. Technol. 160 (2–3) (2002), https://doi.org/10.1016/S0257-8972(02)00415-2.
[111] T. Xin, et al., Phase transformations in an ultralight BCC Mg alloy during anisothermal ageing, Acta Mater. 239 (2022), https://doi.org/10.1016/j.actamat.2022.118248.
[112] J.X. Fang, et al., Transformation-induced strain of a low transformation temperature alloy with high hardness during laser metal deposition, J. Manuf. Process. 68 (2021), https://doi.org/10.1016/j.jmapro.2021.06.066.

[113] Y. Wu, J. Chen, L. Zhang, J. Ji, Q. Wang, S. Zhang, Effect of boron on the structural stability, mechanical properties, and electronic structures of γ′-Ni3Al in TLP joints of nickel-based single-crystal alloys, Mater. Today Commun. 31 (2022), https://doi.org/10.1016/j.mtcomm.2022.103375.
[114] Y.L. Jiang, J.X. Fang, G.Z. Ma, H.L. Tian, D.B. Zhang, Y. Cao, Microstructure and properties of an as-deposited and post treated high strength carbide-free bainite steel fabricated via laser powder deposition, Mater. Sci. Eng., A 824 (2021), https://doi.org/10.1016/j.msea.2021.141791.
[115] Q. Gao, Z. Ding, W.H. Liao, Effective elastic properties of irregular auxetic structures, Compos. Struct. 287 (2022), https://doi.org/10.1016/j.compstruct.2022.115269.